Shell-Model Study of Nuclear Weak Rates relevant to Astrophysical Processes in Stars

Toshio Suzuki[1], Noritaka Shimizu[2], Yusuke Tsunoda[2], Takaharu Otsuka[3,4], and Kenichi Nomoto[5]

[1]Department of Physics, College of Humanities and Sciences, Nihon University Sakurajosui 3-25-40, Setagaya-ku, Tokyo 156-8550, Japan
[2] Center for Computational Sciences, University of Tsukuba, Tennodai 1-1-1, Tsukuba 305-8577, Japan
[3] RIKEN Nishina Center, 2-1 Hirosawa, Wako, Saitama 351-0198, Japan
[4] Department of Physics, The University of Tokyo, Tokyo 113-0033, Japan
[5] Kavli Institute for the Physics and Mathematics of the Universe (WPI), The University of Tokyo, Kashiwa, Chiba 277-8583, Japan

E-mail: [1]suzuki.toshio@nihon-u.ac.jp

Abstract. New shell-model Hamiltonians which can successfully describe spin responses in nuclei are used to evaluate nuclear weak rates in stellar environments. The e-capture and β-decay rates for the nuclear pair with ^{31}Mg-^{31}Al, in the island of inversion, which have been pointed out to be important for the cooling of neutron star crusts, are studied by shell-model calculations with the effective interaction in *sd-pf* shell obtained by the extended Kuo-Krenciglowa (EKK) method. The weak rates induced by the Gamow-Teller transitions between the low-lying states in the nuclear pair lead to a nuclear Urca process. The spin-dipole strengths and e-capture rates for ^{78}Ni are evaluated by shell-model with full *pf-sdg* shells including up to 5p-5h excitations outside filling configurations of ^{78}Ni. The e-capture rates obtained are compared with RPA calculations and the effective rate formula. Weak rates for the second-forbidden transition in ^{20}Ne are evaluated by the multipole expansion method of Walecka as well as the Behrens-Bühring method within *sd*-shell. Difference in the rates between the two methods is found to be rather small as far as the conserved-vector-current (CVC) relation is satisfied. Possible important contributions of the forbidden transition to the heating of the ONeMg core by double e-captures on ^{20}Ne in a late stage of the evolution of the core and implications on the final fate of the core, whether core-collapse or thermonuclear explosion, are discussed.

1. Introduction

Electron-capture and β-decay rates in stellar environments are evaluated by shell-model calculations with the use of Hamiltonians, which can successfully describe spin responses in nuclei. The weak rates induced by Gamow-Teller (GT) transitions are evaluated in *sd*- and *pf*-shell nuclei with the USDB [1] and GXPF1J [2] Hamiltonians, respectively. The weak rates in *sd*-shell are applied to study nuclear Urca processes in ONeMg cores of 8-10M$_\odot$ stars. Electron-capture (β-decay) rates increase (decrease) as the density increases due to the enhancement of the electron chemical potential. Both processes occur simultaneously almost independent of temperature at a certain density, which is referred as a Urca density, and energy is lost from stars by emitting both ν and $\bar{\nu}$. The Urca density is determined by the Q-value for the reactions.

The cooling of the ONeMg core is thus induced mostly by the Urca processes for the ^{23}Na -^{23}Ne and ^{25}Mg -^{25}Na pairs [3, 4].

Accretion of matter to a white dwarf (WD) from the binary companion star occurs in Type-Ia supernovae (SN) for the single-degenerate model. When the WD mass approaches the Chandrasekhar limit, a SN explosion takes place and ^{56}Ni is produced in large amounts. Electron-capture reactions produce neutron-rich isotopes such as ^{58}Ni. A problem of over-production of neutron-excess iron-group isotopes such as ^{58}Ni and ^{54}Cr compared with the solar abundances was noticed when e-capture rates of FFN [5] were used [6]. Now, more accurate e-capture rates obtained by shell-model with GXPF1J and KBF [7] in pf-shell are available. They are generally reduced compared with the FFN rates, and lead to less production of ^{56}Ni etc. Thus, the over-production problem of neutron-rich iron-group elements in Type-Ia SN is suppressed within a factor of $\sim$2 [8, 9].

Here, we evaluate the weak rates for nuclei which concern two-major shells. In Sect. 2, the weak rates for nuclei in the island of inversion, especially the Urca pairs with A=31, are discussed. In Sect. 3, the weak rates for pf-g shell nuclei at neutron number N=50 are treated. In particular, spin-dipole strengths and e-capture rates for ^{78}Ni are evaluated in pf-sdg shell. In Sect. 4, we discuss the second-forbidden transition in ^{20}Ne and the evolution of ONeMg-core toward e-capture SN. The effects of the e-capture on ^{20}Ne on the heating of the core and the final fate of the core, collapse or thermonuclear explosion, are discussed.

2. Weak rates for nuclei in the island of inversion

Nuclear Urca processes for nuclear pairs in the island of inversion have been pointed out to have important roles on the cooling of neutron star crusts [10]. Especially, the ^{31}Al -^{31}Mg pair is among the dominant contributors [11]. Small 2^+ excitation energies and large B(E2) values due to large sd-pf shell admixtures have been found in neutron-rich Ne, Na and Mg isotopes with N -20-22 [12]. The shell gap between neutron $1d_{3/2}$ and $1f_{7/2}$ orbits decreases for nuclei with less protons in $1d_{5/2}$ orbit owing to the shell evolution caused by the tensor interactions: the monopole terms for $\pi d_{5/2}$-$\nu d_{3/2}$ are attractive while those for $\pi d_{5/2}$-$\nu f_{7/2}$ are repulsive [13]. The magic number changes from N=20 to N=16 for neutron-rich isotopes. The number of nucleons in pf-shell excited from sd-shell is found to be around 2 for the SDPF-M Hamiltonian [14], showing the important contributions from 2p-2h excitations. This mechanism is successful in explaining the enhancement of the B(E2) values as well as the reduction of the $2^{;}$ excitation energies in the neutron-rich isotopes with $N \approx$20.

However, the SDPF-M fails to reproduce the energy levels in ^{31}Mg (N=19). The ground state (g.s.) of ^{31}Mg is $1/2^+$, while it is predicted to be $7/2^-$ for the SDPF-M. If the g.s. of ^{31}Mg is taken to be $7/2^-$, the Urca process for the ^{31}Al -^{31}Mg pair hardly occurs as the g.s. of ^{31}Al is $5/2^+$ and the g.s.-g.s. transition is forbidden.

A new method for obtaining effective interactions in non-degenerate two-major shells has been proposed [15, 16]. The method, referred as the extended Kuo-Krenciglowa (EKK) method, can avoid the divergence problem in the energy denominator in the Q-box expansions by introducing an energy parameter. An effective interaction in sd-pf shell, EEdf1 [17], has been constructed by the EKK method starting from a chiral EFT interaction N^{3}LO [18] and the three-nucleon forces of Fujita-Miyazawa [19]. The energy levels in 31Mg are successfully reproduced with $1/2^+$ for the g.s. and $3/2^+$ for the first excited state. The EEdf1 leads to more sd-pf shell admixtures than the SDPF-M: the 4p-4h components is found to be comparable to the 2p-2h components in ^{32}Mg [16]. The 2p-2h and 4p-4h components in the g.s. of ^{31}Mg (^{31}Al) are found to be 66% (43%) and 30% (13%), respectively. The e-capture and β-decay rates for the ^{31}Al -^{31}Mg pair in the stellar environments are shown in Fig. 1. Dominant contributions to the weak rates for the A=31 pair come from the GT transitions, ^{31}Al ($5/2^+$) $\leftrightarrow$ ^{31}Mg ($3/2^+$, 0.050 MeV), thus leading to a nuclear Urca process.

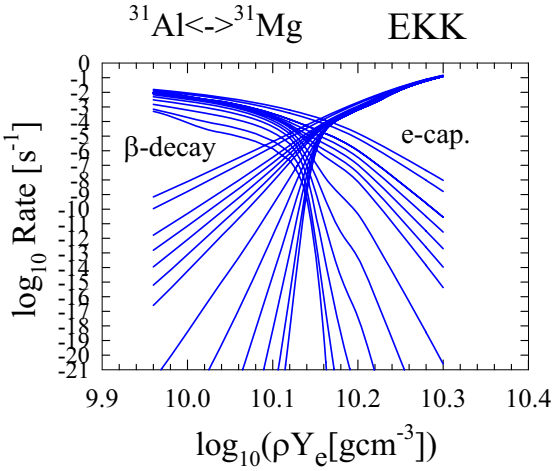

Figure 1. (Left figure) Electron-capture and β-decay rates obtained by shell-model calculations in *sd-pf* shell with the EEdf1 interaction [16]. Figure taken from Ref. [20].

3. Electron-capture rates for ^{78}Ni

In this section, we discuss the weak rates of *pf-g* shell nuclei in the N=50 region, which have been shown to be important for the core-collapse processes in the SN explosions [21]. Here, spin-dipole strengths and e-capture rates in ^{78}Ni are evaluated with the extended version [22] of the modified A3DA interaction [23]. Configurations up to 5p-5h excitations outside the closed ^{78}Ni-core are taken into account in the full *pf-sdg* shell, that is, with $g_{9/2,7/2}, d_{5/2,3/2}$ and $s_{1/2}$ shells. Calculated spin-dipole strengths are shown in Fig. 2(a). The largest contributions come from excitations of 1^- states. The sum of the strengths for the present shell-model calculations exhaust 95%, 96% and 79% of the total strengths of 0^-, 1^- and 2^-, respectively. An extension beyond 5p-5h excitations is preferred to improve the situation in 2^- as well as to treat deformed intruder states. The e-capture rates are evaluated with the multipole expansion method of Walecka [24, 25] as well as the Behrens-Bühring method [26, 27, 20]. The e-capture rates for finite density and temperature in the Walecka method are given as [24, 25]

$$\begin{aligned} \lambda^{ecap}(T) &= \frac{V_{ud}^2 g_V^2 c}{\pi^2(\hbar c)^3}\int_{E_{th}}^{\infty}\sigma(E_e,T)E_e p_e c S_e(E_e)dE_e \\ \sigma(E_e,T) &= \sum_i \frac{(2J_i+1)e^{-E_i/kT}}{G(Z,A,T)}\sum_f \sigma_{f,i}(E_e) \end{aligned} \quad (1)$$

where $V_{ud}=\cos\theta_C$ is the up-down element in the Cabibbo-Kobayashi-Maskawa quark mixing matrix with θ_C the Cabibbo angle, $g_V=1$ is the weak vector coupling constant, E_e and p_e are electron energy and momentum, respectively, E_{th} is the threshold energy for the electron capture, and $S_e(E_e)$ is the Fermi-Dirac distribution for the electron, and $G(Z,A,T)=\sum_i(2J_i+1)e^{-E_i/kT}$. The cross section $\sigma_{f,i}(E_e)$ from an initial state with E_i and spin J_i to a final state with excitation energy E_f and spin J_f is evaluated with the multipole expansion method [24, 25] as follows:

$$\begin{aligned} \sigma_{f,i}(E_e) &= \frac{G_F^2}{2\pi}F(Z,E_e)W(E_\nu)C_{f,i}(E_e) \\ C_{f,i}(E_e) &= \frac{1}{2J_i+1}\int d\Omega(\sum_{J\geq 1}\{(1-(\hat{\vec{\nu}}\cdot\hat{\vec{q}})(\vec{\beta}\cdot\hat{\vec{q}})[|\langle J_f||T_J^{mag}||J_i\rangle|^2+|\langle J_f||T_J^{elec}||J_i\rangle|^2] \\ &- 2\hat{\vec{q}}\cdot(\hat{\vec{\nu}}-\vec{\beta})Re\langle J_f||T_J^{mag}||J_i\rangle\langle J_f||T_J^{elec}||J_i\rangle^*\} \end{aligned}$$

$$+ \sum_{J\geq 0}\{(1-\hat{\vec{\nu}}\cdot\vec{\beta})+2(\hat{\vec{\nu}}\cdot\hat{\vec{q}})(\vec{\beta}\cdot\hat{\vec{q}})|\langle J_F||L_J||J_i\rangle|^2+(1+\hat{\vec{\nu}}\cdot\vec{\beta})|\langle J_f||M_J||J_i\rangle|^2$$
$$- 2\hat{\vec{q}}\cdot(\hat{\vec{\nu}}+\vec{\beta})Re\langle J_f||L_J||J_i\rangle\langle J_f||M_J||J_i\rangle^*\}), \quad (2)$$

where $\vec{q}=\vec{\nu}-\vec{k}$ is the momentum transfer with $\vec{\nu}$ and $\vec{k}$ the neutrino and electron momentum, respectively, $\hat{\vec{q}}$ and $\hat{\vec{\nu}}$ are the corresponding unit vectors and $\vec{\beta}=\vec{k}/E_e$. G_F is te Fermi coupling constant, $F(Z,E_e)$ is the Fermi function, and $W(E_\nu)$ is the neutrino phase space factor given by $W(E_\nu)=\frac{E_\nu^2}{1+E_\nu/M_T}$, where $E_\nu=E_e+Q+E_i-E_f$ is the neutrino energy with E_i and E_f the excitation energies of initial and final nuclear states, respectively, and M_T is the target mass. The Q value is determined from $Q=M_i-M_f$, where M_i and M_f are the masses of parent and daughter nuclei, respectively. The Coulomb, longitudinal, transverse magnetic and electric multipole operators with multipolarity J are denoted as M_J, L_J, T_J^{mag} and T_J^{elec}, respectively.

The shape form factors for the e-capture processes with $\lambda^\pi=0^-$, 1^- and 2^- are given as follows in the low-momentum transfer limit:

$$\begin{aligned} C_{ecap}^{0^-} &= (\xi' v-\frac{1}{3}wW_0)^2 \\ C_{ecap}^{1^-} &= [\xi' y+\frac{1}{3}(u+x)W_0]^2+\frac{1}{18}(u-2x)^2 \\ &+ W[-\frac{4}{3}\xi' yu-\frac{W_0}{9}(4x^2+5u^2)]+\frac{W^2}{9}(4x^2+5u^2) \\ C_{ecap}^{2^-} &= \frac{1}{3}z^2(W_0-1)^2 \end{aligned} \quad (3)$$

where

$$\begin{aligned} \xi' v &= -\frac{\sqrt{3}}{\sqrt{2J_i+1}}g_A<f||\frac{1}{M}[\vec{\sigma}\times\vec{\nabla}]^{(0)}||i>, \quad w=-\frac{\sqrt{3}}{\sqrt{2J_i+1}}g_A<f||r[C^1(\Omega)\times\vec{\sigma}]^{(0)}||i> \\ \xi' y &= \frac{1}{\sqrt{2J_i+1}}<f||\frac{\vec{\nabla}}{M}||i>, \qquad\qquad x=\frac{1}{\sqrt{2J_i+1}}<f||rC^1(\Omega)||i> \\ u &= \frac{\sqrt{2}}{\sqrt{2J_i+1}}g_A<f||r[C^1(\Omega)\times\vec{\sigma}]^{(1)}||i>, \quad z=\frac{1}{\sqrt{2J_i+1}}g_A<f||r[C^1(\Omega)\times\vec{\sigma}]^{(2)}||i> \end{aligned} \quad (4)$$

with W the electron energy ($=E_e$), $W_0=|Q|$ where Q is the Q-value for the reaction, and J_i is the angular momentum of the initial state. The relation, $\xi' y$ =-$\Delta E_{fi}x$ with $\Delta E_{fi}=E_f-E_i$, is satisfied because of the conserved-vector current (CVC). Here, the $\xi' y$ term is obtained by just performing derivative of wave functions. In this case, ΔE_{fi} is equal to 1 (-1) $\hbar\omega$ for pf $(sdg)\rightarrow$ sdg (pf) transitions in each matrix element when harmonic oscillator wave functions are used.

Calculated e-capture rates obtained by the shell-model are shown in Fig. 2(b), and compared with those by the effective rate formula and random-phase-approximation (RPA). The effective rate formula [21] has two parameters, the effective transition strength and effective energy difference ΔE, that modifies the Q-value to Q -ΔE. The value of ΔE denotes the excitation energy for the effective peak position of the transition strength. A value of ΔE =2.5 MeV adopted in the effective rate formula is close to the effective peak position of the strength obtained by the shell-model. The e-capture rates for the shell-model are thus close to those by the effective rate formula. The rates for the RPA are smaller than the shell-model rates as the strengths for the RPA are shifted toward higher energy region.

In the Behrens-Bühring (BB) method, distorted electron wave functions are used, which results in extra interference terms between the operators and the electron wave functions (see Refs. [20, 26] for the details). In the present e-capture rates induced by the first-forbidden transitions, the effects of the electron distortion on the rates are found to be as small as about 20% [20].

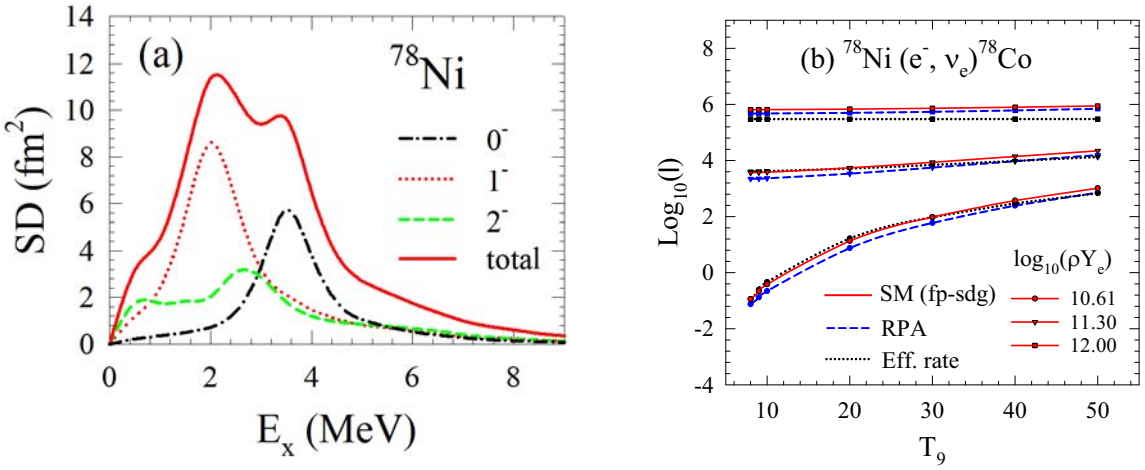

Figure 2. (a) Spin-dipole strengths for ^{78}Ni obtained by shell-model calculations in *pf-sdg* shell with the extended version [22] of the modified A3DA interaction [23]. (b) Calculated e-capture rates for ^{78}Ni obtained by shell-model, RPA and the effective rate formula. Here, the axial-vector coupling constant is taken to be a free value, g_A =-1.26. Figures taken from Ref. [20].

4. Second-forbidden transitions in ^{20}Ne and evolution of ONeMg-core toward e-capture supernovae

An unexpected large contribution from the second-forbidden transition in ^{20}Ne to the e-capture rates was pointed out at $\log_{10}(\rho Y_e) = 9.2$-$9.6$ and $\log_{10}$ (T) $\leq$8.8, and evaluated as an allowed GT transition with log $ft = 10.5$ [28]. The β-decay rate from ^{20}F ($2^+_{g.s.}$) was recently measured; log ft =10.89(11) [29]. The forbidden transition with $J\,\pi = 2^+$ has Coulomb (C_2), longitudinal (L_2), transverse electric (T_2^{elec}) and axial magnetic (M_2^5) form factors.

In the low momentum transfer (q) limit, the shape factor is given as

$$\begin{aligned} C(k,\nu) &= \frac{1}{45}x^2(k^4 - \frac{4}{3}\beta k^3\nu + \frac{10}{3}k^2\nu^2 - \frac{4}{3}\beta k\nu^3 + \nu^4) + \frac{2}{15}y^2(k^2 - 2\beta k\nu + \nu^2) \\ &+ \frac{2}{45}\sqrt{6}xy(\beta k^3 - \frac{5}{3}k^2\nu + \frac{5}{3}\beta k\nu^2 - \nu^3) \\ &+ \frac{1}{5}y^2(k^2 + \nu^2 + \frac{4}{3}\beta k\nu) + \frac{1}{45}u^2(k^4 + 2\beta k^3\nu + \frac{10}{3}k^2\nu^2 + 2\beta k\nu^3 + \nu^4) \\ &- \frac{2}{15}yu(\beta k^3 + \frac{5}{3}k^2\nu + \frac{5}{3}\beta k\nu^2 + \nu^3). \end{aligned} \quad (5)$$

with k the electron momentum, $\beta = k/E_e$, and ν the neutrino energy, and

$$\begin{aligned} x &= \frac{1}{\sqrt{2J_i+1}}\langle J_f||\sum_k r_k^2 C^2(\Omega_k)||J_i\rangle \\ y &= \frac{1}{\sqrt{2J_i+1}}\langle J_f||\sum_k r_k[C^1(\Omega_k)\times\frac{\vec{\nabla}_k}{M}]^2||J_i\rangle \\ u &= \frac{1}{\sqrt{2J_i+1}}g_A\langle J_f||\sum_k r_k^2[C^2(\Omega_k)\times\vec{\sigma}_k]^2||J_i\rangle \end{aligned} \quad (6)$$

with $C^\lambda = \sqrt{\frac{4\pi}{2\lambda+1}}Y^\lambda$. The matrix elements x, y and u correspond to C_2, L_2 or T_2^{elec}, and M_2^5, respectively.

In the limit of $q \to 0$,

$$L_2(q) = \sqrt{\frac{2}{3}}T_2^{elec} = -\frac{i}{q}\sum_k \frac{q^2 r_k^2}{15}\vec{\nabla}\cdot\vec{V}_{\pm,k}Y\ 2(\Omega), \tag{7}$$

where $\vec{V_\pm}$ is the charged weak vector current.

The CVC relation

$$\vec{\nabla}\cdot\vec{V}_\pm = -\frac{\partial\rho_\pm}{\partial t} = -i[H,\rho_\pm] \tag{8}$$

where $\rho_\pm = F_1^V(q^2)\sum_k \vec{\delta}(\vec{r}-\vec{r}_k)t_\pm$ is the time component of $V_\pm$ and H is the total Hamiltonian of the nucleus, leads to

$$\begin{aligned}\langle J_f||L_2(q)||J_i\rangle &= \sqrt{\frac{2}{3}}\langle J_f||T_2(q)||J_i\rangle = -\frac{E_f-E_i}{q}\langle J_f||C_2(q)||J_i\rangle,\\ y &= -\frac{E_f-E_i}{\sqrt{6}\hbar}x.\end{aligned} \tag{9}$$

With the inclusion of the isovector electromagnetic interaction [30], the energy difference is modified to include the isovector part of the electromagnetic interaction rotated into the $\pm$ direction in isospin space, that is, the Coulomb energy difference V_C, and the neutron-proton mass difference [31],

$$\Delta E \equiv E_f - E_i \pm V_C \mp (m_n - m_p). \tag{10}$$

ΔE becomes the energy of the IAS of ^{20}F ($2^+_{g.s.}$), tha is, ^{20}Ne (2^+, T=1, 10.724 MeV).

In case of the Behrens-Bühring (BB) method, electron distorted wave in a Coulomb potential gives rise to interference terms between the operators and the distorted waves [26, 20]. Calculated shape factor for the second-forbidden transition in ^{20}Ne as well as the total capture rates including the GT transitions obtained with the USDB are shown in Fig. 3.

While the important role of the CVC relation is noticed, the difference between the Walecka and BB methods are rather small as far as the CVC is taken into account for the E2 matrix element. Note that the shape factor depends on the electron energy in contrast to the cases in which the transition is treated as am allowed GT one. The contributions from the forbidden transition to the capture rates become important at $\log_{10}(\rho Y_e)$ =9.4-9.65 as shown in Fig. 3(b). The present results with the CVC relation are consistent with those of Ref. [29].

Now, we discuss the heating of the ONeMg core by double e-capture processes, ^{20}Ne (e$^-$, ν_e) ^{20}F (e$^-$, ν_e) ^{20}O. The e-capture on ^{20}F takes place immediately after the e-capture on ^{20}Ne as the threshold energy for the e-capture on the odd-odd nucleus ^{20}F is smaller than the first one because of the pairing effects. The core is heated by γ emissions from excited states of ^{20}O.

The double e-captures on ^{20}Ne occurs just before the Urca process for the ^{25}Na -^{25}Ne pair takes place, and leads to the heating of the core. The evolution of the star with 8.4M$_\odot$ have been studied [32] using the MESA code [33]from the main sequence till the oxygen ignition, where the energy production becomes equal to the ν energy loss. The weak rates denoted as USDB in Fig. 3(b) [34] have been used. The core evolves through complicated processes of mass accretion, heating by e-capture, cooling by Urca processes, and Y_e change. The location of the oxygen ignition (center or off-center) and the Y_e distribution depend on the input physics and the treatment of the semiconvection and convection. The core density of the oxygen ignition, $\rho_{c,ign}$, is around $\log_{10}(\rho_{c,ign}/\mathrm{g\ cm^{-3}}) = 9.96$-10.0. The oxygen deflagration is expected to occur at the core density, $\rho_{c,def}$, higher than $\rho_{c,ign}$ due to the convection effects. Since the oxygen

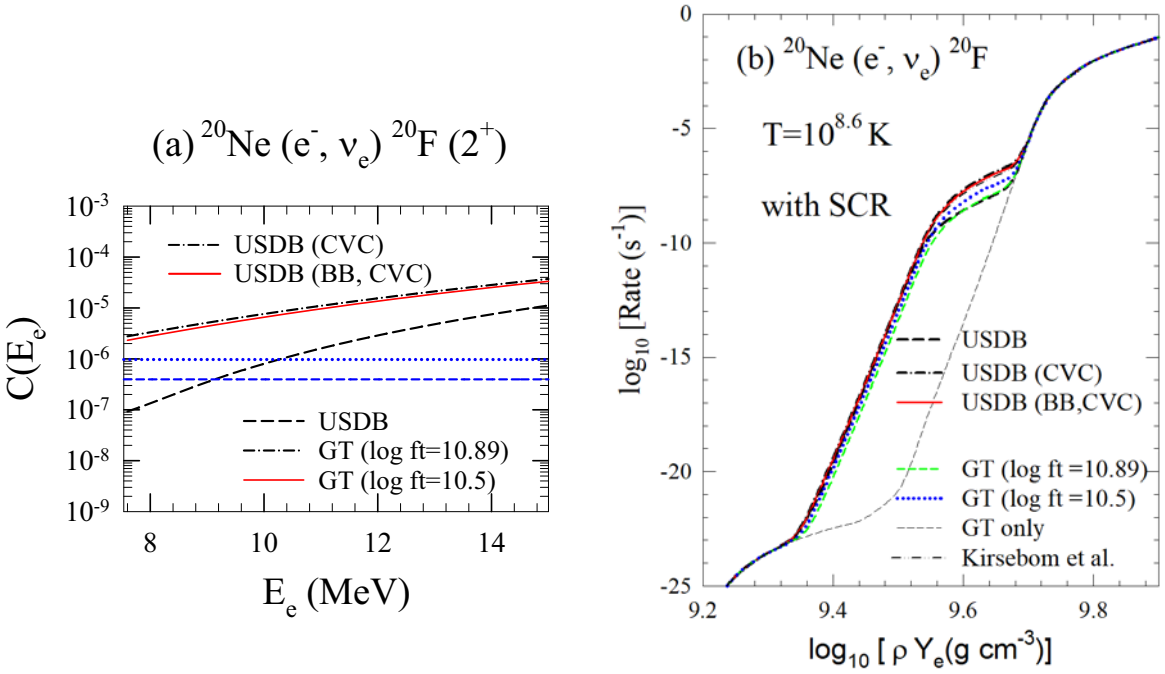

Figure 3. (a) Shape factors for the second-forbidden transition in ^{20}Ne. (b) Calculated total e-capture rates for ^{20}Ne with both the GT and the forbidden transitions. USDB (CVC) and USDB are obtained with and without the CVC relation for the evaluation of the transverse E2 matrix elements, respectively, by the Walecka method, while USDB (BB, CVC) are obtained with the BB method with the CVC relation. GT denotes that they are obtained as an allowed GT transition with the strength determined from the log ft values. The rates in Ref. [29] are also shown. Figures taken from Ref. [20].

burning occurs at $T \sim 10^{9.3}$ K, $\rho_{c,def}$ is estimated to be $\rho_{c,def} > 10.10$ g cm^{-3} [32], and $\rho_{c,def} = 10.2$ g cm^{-3} in Ref. [35].

To examine the final fate of the ONeMg core, 2D hydrodynamical simulations for the propagation of the oxygen deflagration wave have been performed for various initial conditions for the deflagration [32]. Three cases of Y_e distributions, three locations of the oxygen ignition (center, off-center at r_{ign} = 30 km and 60 km), and various central densities at $\log_{10}(\rho_{c,def}/\mathrm{g\ cm^{-3}})$ =9.96-10.2 are used for the initial configurations at the initiation of the deflagration. The central density for the explosion-collapse bifurcation is found to be at $\log_{10}(\rho_{crt}/\mathrm{g\ cm^{-3}})$ =10.01 [32]. Since $\log_{10}(\rho_{c,def})$ is estimated to be above 10.1 and exceeds this critical value, the ONeMg core is likely to collapse to form a NS, though further studies of the convection and semiconvection before the deflagration are needed. It would be interesting to see if the present conclusion remains valid for the rates with the CVC relation, denoted as USDB (CVC) and USDB (BB, CVC) in Fig. 3(b).

Jones et al. [36] with the rates GT (log ft=10.50) and Kirsebom et al. [29] with the rates USDB (BB, CVC), on the other hand, obtained the opposite conclusion in favor of thermonuclear explosion by assuming that the effects of convection and semiconvection would be small, that is, $\rho_{c,def} \approx \rho_{c,ign} \approx 9.96$-9.97. Investigations whether the convective energy transport is efficient enough to delay the ignition and the start of the oxygen deflagration wave to densities above the critical density for collapse were left for the future. In case of thermonuclear explosions, the oxygen deflagration results in a partial disruption of the ONeMg core with an ONeFe WD left

behind [36].

It is not easy to find clear evidence for thermonuclear ECSN (tECSN) or collapsing ECSN (cECSN). In tECSN, ONeFe WD is expected to be formed as a remnant. Information on its mass-radius relation could assign ONeFe WD [37]. In Ref. [38], SN2018zd is shown to have strong evidence for or consistent with various indicators of e-capture supernovae, that is, progenitor identification, circumstellar material, chemical composition, explosion energy, light curve and nucleosynthesis. Theoretically, we need to understand more clearly the evolution from the oxygen ignition (at the end of the MESA calculations) till the beginning of the deflagration by taking into account the semiconvection and convection. More observational and theoretical studies are desirable to be done to draw a definite conclusion on the final fate of the stars with 8-10 $M_{\odot}$, whether cECSN or tECSN.

The author would like to thank N. Tsunoda, S. Zha, and S.-C. Leung for collaboration of the works presented here. This work has been supported in part by JSPS KAKENHI Grant No. JP19K03855.

[1] Brown B A and Richter W A 2006 *Phys. Rev.* C **74** 034315
Richter W A, Mkhize S and Brown B A 2008 ibid. **78** 064302
[2] Honma M, Otsuka T, Mizusaki T, Hjorth-Jensen M and Brown B A 2005 *J. Phys. Conf. Ser.* **20** 7
[3] Toki H, Suzuki T, Nomoto K, Jones S and Hirschi R 2013 *Phys. Rev.* C **88** 015806
[4] Suzuki T, Toki H and Nomoto K 2016 *Astrophysical J.* **817** 163
[5] Fuller G M, Fowler W A and Newman M J 1980 *Astrophysical J.* Suppl. **42** 447; ibid 1982 **252**, 715; ibid Suppl. 1982 **48**, 279
[6] Iwamoto K et al 1999 *Astrophys. J. Suppl.* **125** 439
[7] Langanke K and Martínez-Pinedo G 2001 *At. Data and Nucl. Data Tables* **79** 1
[8] Mori K, Famiano M A, Kajino T, Suzuki T et al 2016 *Astrophys. J.* **833** 179
[9] Mori K, Suzuki T, Honma M, Famiano M A, Kajino T, Kusakabe M and Balantekin A B 2020 *Astrophys. J.* **904** 29
[10] Schatz H et al 2014 **Nature 505** 62
[11] Ong W-J et al 2020 *Phys. Rev. Lett.* **125** 262701
[12] Warburton E K, Becker J A and Brown B A 1990 *Phys. Rev. C* **41** 1147
[13] Otsuka T, Suzuki T, Fujimoto R, Grawe H and Akaishi Y 2005 *Phys. Rev. Lett.* **95** 232502
[14] Utsuno Y, Otsuka T, Mizusaki T and Honma M 1999 *Phys. Rev.* C **60** 054315
[15] Takayanagi K 2011 *Nucl. Phys. A* **852** 61; ibid. 2011 **864** 91
[16] Tsunoda N, Otsuka T, Shimizu N, Hjorth-Jensen M, Takayanagi K and Suzuki T 2017 *Phys. Rev. C* **95** 021304
[17] Otsuka T, Gade A, Sorlin O, Suzuki T and Utsuno Y 2020 *Rev. Mod. Phys.* **92** 015002
[18] Machleidt R and Entem D R 2011 *Phys. Rep.* **503** 1
[19] Fujita J and Miyazawa H 1957 *Prog. Theor. Phys.* **17** 360
[20] Suzuki T 2022 *Prog. in Part. Nucl. Phys.* **126** 103974
[21] Sullivan C, OConnor, E, Zegers R G T, Grubb T and Austin S M 2016 *Astrophysical J.* **816** 40
[22] Taniuchi R, Santamaria C, Doornenbal P et al 2019 *Nature* **569** 53
[23] Tsunoda Y, Otsuka T, Shimizu N, Honma M and Utsuno Y 2014 *Phys. Rev. C* **89** 031301 (R)
[24] Walecka J D in *Muon Physics*, Vol. II, ed. Hughes V W and Wu C S (New York, Academic, 1975)
[25] O'Connell J S, Donnelly T W and Walecka J D 1972 *Phys. Rev. C* **6** 719
[26] Behrens H and Bühring W 1971 **Nucl. Phys. A 162** 111
[27] Schopper H *Weak Interactions and Nuclear Beta Decays* (North-Holland, Amsterdam, 1966)
[28] Martínez-Pinedo G, Lam Y H, Langanke K, Zegres R G, Sullivan C 2014 *Phys. Rev. C* **89** 045806
[29] Kirsebom O S et al 2019 *Phys. Rev. Lett.* **123** 262701; 2019 *Phys. Rev. C* **100** 065805
[30] Blin-Stoyle R J *Fundamental Interactions and the Nucleus* (North-Holland, Amsterdam, 1973)
[31] Fujita J 1962 *Phys. Rev.* **126** 202; 1962 *Prog. Theor. Phys.* **28** 338
[32] Zha S, Leung S-C, Suzuki T and Nomoto K 2019 **Astrophysical J. 886** 22
[33] Schwab J and Rocha K A 2019 *Astrophysical J.* **872** 131
[34] Suzuki T, Zha S, Leung S-C, Nomoto K 2019 *Astrophysical J.* **881** 64
[35] Takahashi K, Sumiyoshi K, Yamada S, Umeda H and Yoshida T 2019 *Astrophysical J.* **871** 153
[36] Jones S, Ropke F K, Pakmor R et al 2016 *Astronomy and Astrophysics* **593** A72
[37] Jones S, Ropke F K, Fryer C et al 2019 *Astronomy and Astrophysics* **622** A74
[38] Hiramatsu D, Howell D A, Van Dyk S D et al 2021 *Nature Astronomy* **5**